

Silver Electrolysis for Disinfection of Spacecraft Potable Water: 2024 Update

Phillip M. Hicks[1], Rogelio Garcia Fernandez[1]
Jacobs Technology, Houston, TX, 77058, U.S.A.

and

Niklas Adam[2]
NASA Johnson Space Center, Houston, TX, 77058, U.S.A.

Anodic dissolution of silver electrodes, or "silver electrolysis," is being investigated as a means of introducing biocidal silver into potable water on exploration spacecraft. This paper provides an update on the effort to implement this technology into a spacecraft potable water system. Previous papers reported on the feasibility of the technology for this application, strategies to prevent a potential fault condition termed "electrode bridging," results from a preliminary investigation into the cathode reaction, and preliminary multiphysics modeling of the reactor. Since then, work has begun on the design of a next-generation silver electrolysis reactor prototype that will incorporate improvements identified in previous testing and package the reactor in a more flight-like configuration. This development effort has included additional testing to optimize the reactor design for prevention of electrode bridging, further investigation into the cathode reaction (including the use of a dissolved hydrogen sensor), and an assessment of the feasibility of using the reactor in other applications, such as for microbial shock and preparation for system dormancy.

Nomenclature

Ag_k	=	silver concentration, calculated based on conductivity measurement (see Ref. 1)
C	=	mass-based concentration
CR01	=	Cathode Reaction (Test) 01
DI	=	deionized
DO	=	dissolved oxygen
DORB	=	dissolved oxygen removal bed
F	=	Faraday's constant
I	=	current
IC	=	ion chromatography
ISE	=	ion-selective electrode
IX	=	ion exchange
κ, k	=	conductivity
mA	=	milli-amp
µA/cm^2	=	micro-amp per centimeter squared
mg/L	=	milli-grams per liter solution
µS/cm	=	micro-Siemens per centimeter
v	=	stoichiometric ratio
φ_i	=	current fraction of reaction i (see also Table 1)
PC	=	polycarbonate
ppb	=	part per billion
PTFE	=	polytetrafluoroethylene
TOC	=	total organic carbon
$\dot{V}$	=	volumetric flowrate

[1] Project Engineer, Jacobs Technology – JETS II Contract, Jacobs Engineering (2224 Bay Area Blvd)
[2] Water Technology Engineer, Crew and Thermal Systems Division, Mail Stop: EC3 (2101 NASA Pkwy)

I. Introduction

Ionic silver at concentrations between 200–400 ppb is being considered as a replacement for iodine as the residual biocide in future spacecraft potable water systems. Specifically, a silver-ion-imparting technology is sought to replace the iodine-imparting resin in the product water segment of the water processor. Replacing iodine with silver requires an in-line method to accurately introduce the silver into water under conditions expected in a spacecraft water processor, which include low conductivity and low flowrate. Furthermore, the method should require little to no maintenance (including replacement of consumables) over the duration of a three-year mission. Finally, it must have reasonably low mass and volumetric footprint.

Silver electrolysis is a promising candidate technology for this purpose as it can be controlled and monitored via simple electrical parameters, it requires no moving parts, and it does not rely on a chemical resin that is depleted over time. Feasibility testing that was reported in a prior paper[1] demonstrated the capability of a silver electrolysis system to deliver a consistent silver concentration for a long duration and monitor the concentration via conductivity measurement. This testing represented a major milestone in the development of the electrolytic silver dosing technology. However, it also uncovered a fault condition that occurs in some reactor configurations and modes of operation. The fault occurs when silver deposits on interelectrode surfaces (the nonconducting, wetted material that the electrodes sit on and/or are held in place by) and forms a conductive "bridge" between electrodes, resulting in diminished silver output. Subsequent testing (reported last year[2]) demonstrated two strategies that are very effective for preventing the bridging fault: 1) increasing the frequency of polarity reversal (from every thirty minutes to every one minute) and 2) masking the edges of the electrodes that are in contact with the interelectrode surfaces. These strategies were both effective independently, but both exhibited room for improvement.

Periodically switching polarity reverses the unwanted reactions that take place on the electrodes. It combats electrode bridging by reversing the cathodic silver deposition that tends to grow on interelectrode surfaces across the electrode gap. A polarity reversal frequency of thirty minutes slowed this process but did not eliminate the bridging fault. With increased reversal frequency (1 minute half-cycles), deposits still formed, but only along the electrode edges: the deposits did not grow across the gap and thus appeared to pose no risk of electrode bridging. However, it was desired to determine whether those deposits could be eliminated altogether. To that end, testing of alternate interelectrode materials was conducted to determine if lower surface energy would inhibit direct bonding of the deposit or if lower porosity would inhibit deposit anchoring into the surface. Teflon PTFE was chosen as representative of materials with low surface energy, and quartz was chosen as representative of materials with low porosity. This test is discussed in Section IIIA.

Masking of the electrode edges independently prevented electrode bridging and formation of silver deposits (i.e. it was effective without reversing polarity), but silver dendrites eventually began to form at the active (unmasked) surface of the cathode. Upon reaching a critical size, these dendrites would detach from the cathode, resulting in flakes that were then carried downstream.[2] It was concluded that a combination of edge masking and polarity reversal should yield optimal performance. Furthermore, in prior testing, electrode edges were masked with electroplating tape. A more permanent solution was sought in the form of a polymeric coating that could be selectively applied to the edges of the electrodes. The coating must prevent the penetration of ionic silver to the electrode substrate, which is the same requirement levied on coatings for silver loss prevention, which has been extensively studied. Work by Vance, et al, has shown that parylene-C* is an effective coating for preventing loss of ionic silver to traditional spacecraft plumbing materials, especially 316L stainless steel.[3-6] Furthermore, a broad survey of polymeric coatings on 316L stainless steel, Titanium Grade 2, and Inconel 718 concluded that there are several coatings that effectively prevent penetration of silver ions and thus loss of ionic silver from solution.[7] Subsequent, preliminary results from this group showed that, of these coatings, parylene-C provided the best combination of prevention of silver ion penetration and low leaching of contaminants (based on total concentration of non-silver ionic species). Parylene-C was thus selected as the first coating to test as an electrode edge masking material. Although parylene-C has been used in many diverse applications, this is the first time that the authors (and the vendor) are aware of that the coating has been used as an electrode mask in an electrolysis reactor. Thus, the coating was tested to ensure its suitability for the application. Specific test objectives included 1) confirming long-term performance of the reactor with edge-coated electrodes, 2) determining whether any contaminants (especially organics) are leached from the coating during both quiescent timeframes and during (or as a result of) electrolysis, and 3) determining whether any degradation of the

*Parylene is the generic name for a series of polymeric conformal coatings comprising poly(para-xylylene); the "-C" variant replaces one of the aromatic hydrogens with a chlorine atom.[8]

coating or its adhesion to the electrode results from electrolysis and/or long-duration exposure to water. This test is described in Section IIIB.

Last year's paper also reported on the impact of influent dissolved oxygen (DO) concentration on reactor performance. Specifically, it was found that the cathode reaction is impacted by DO concentration. Although the primary anode reaction (silver dissolution) is the purpose of the reactor, the cathode reaction is an essential part of any electrochemical process and must be considered when investigating the overall performance of the system. Furthermore, an understanding of the cathode reaction(s) yields insight into the anode reaction(s). Possible electrode reactions[†] are shown in Table 1.

Table 1. Electrode Reactions

Electrode	Reaction	Description	Abbreviation
Anode	$Ag \rightarrow Ag^+ + e^-$	Silver dissolution	Ag+
	$Ag + OH^- \rightarrow \frac{1}{2}Ag_2O + \frac{1}{2}H_2O + e^-$	Oxide formation	Ag2O
Cathode	$\frac{1}{4}O_2 + \frac{1}{2}H_2O + e^- \rightarrow OH^-$	Oxygen reduction	O2
	$H_2O + e^- \rightarrow \frac{1}{2}H_2 + OH^-$	Hydrogen evolution	H2
	$Ag^+ + e^- \rightarrow Ag$	Silver deposition	Ag_dep

Given the purity of the water processor product water, the only reducible species in the reactor electrolyte are dissolved oxygen, hydronium ions,[‡] and silver ions that have migrated from the anode. Thus, the primary cathode reaction is either reduction of dissolved oxygen (DO) or evolution of hydrogen, with a likely secondary reaction being the reduction of ionic silver (silver deposition). Oxygen reduction is the thermodynamically favored reaction, but kinetic limitations of this reaction may permit the hydrogen evolution reaction to proceed instead. Last year's data showed that dissolved oxygen consumption is the primary cathode reaction and that the influent dissolved oxygen concentration has negligible impact on reactor performance when it is in the range expected in water processor product water (>5.5 mg/L).[2] It was suspected that the hydrogen evolution reaction took over as the primary cathode reaction at very low DO concentrations. To test that hypothesis, a dissolved hydrogen sensor was added to the test rig for what was dubbed the Cathode Reaction Test. This test is described in Section IIIC.

Finally, there are specific applications in which a silver electrolysis reactor may need to be operated in different regimes. For example, an advantage of the technology is its ability to dose higher concentrations by simply increasing the current. This ability would be very useful in the event that a higher starting concentration is desired for dormancy or a high-concentration shock is required to respond to microbial contamination in any water system. For this reason, the reactor was tested at higher currents to ascertain the maximum achievable silver concentration in a given reactor configuration. This Elevated Concentration Test is discussed in Section IIID. Each of these efforts are part of a continuing campaign to develop a flight-ready electrolytic silver biocide dosing system in support of NASA's future exploration goals.

II. Methods

The test article, test rig, and execution of each test is summarized in Table 2 and described in detail in the following subsections.

A. Test Article (Reactor)

The silver electrolysis reactor proof-of-concept prototype (hereafter "reactor") that was used in prior testing[1-2] was also used for this test program. The reactor body consists of a polycarbonate base and lid that can be separated to allow the insertion of a variable number of parallel plate silver electrodes and interchangeable electrode-spacing components. The electrodes protrude through the reactor lid to enable electrical connection with quick-disconnect flag receptacles. The non-permanent nature of the water seal and electrical connection permit the electrodes to be

[†]Other silver oxides with higher silver oxidation state are possible,[9] but Ag_2O is the most thermodynamically likely, and other oxides would have the same impact on reactor performance. Thus, in this paper, Ag_2O is considered representative of silver oxides in general.

[‡] In alkaline solution, the hydronium ions originate from the dissociation of water. The hydrogen evolution reaction in Table 1 is written in the alkaline form, such that water is the reducible species in that reaction.

Table 2. Test Methods

Test*	Spacer Config	# Electrodes	Electrode Mask	Test Rig Includes	Flowrate (mL/min)	Current (mA)	Polarity Reversal
Alt. Intelec. Matl. 01	01	2	None	B,D	33	0.33	None
Alt. Intelec. Matl. 02	01	2	None	B,D	33	0.7	1 min
Coated Edge	02	2	Parylene-C	B,D	33	0.5	1 min
Cathode Reaction 01	02	10	Electroplating tape	A,B,C	100	0.75	See text
Cathode Reaction 02	02	10	Electroplating tape	A,B,C	100	3	See text
Cathode Reaction 03	02	2	Electroplating tape	A,B,C	100	0.75	See text
Elevated Conc. 01	02	10	Electroplating tape	B,D	100	1.5 - 9.0	See text
Elevated Conc. 02	02	10	Electroplating tape	D	100	1.5 - 9.0	See text

*The number after a test name indicates the test case. Note that some test cases had several steps or iterations, as described in Section IIC.

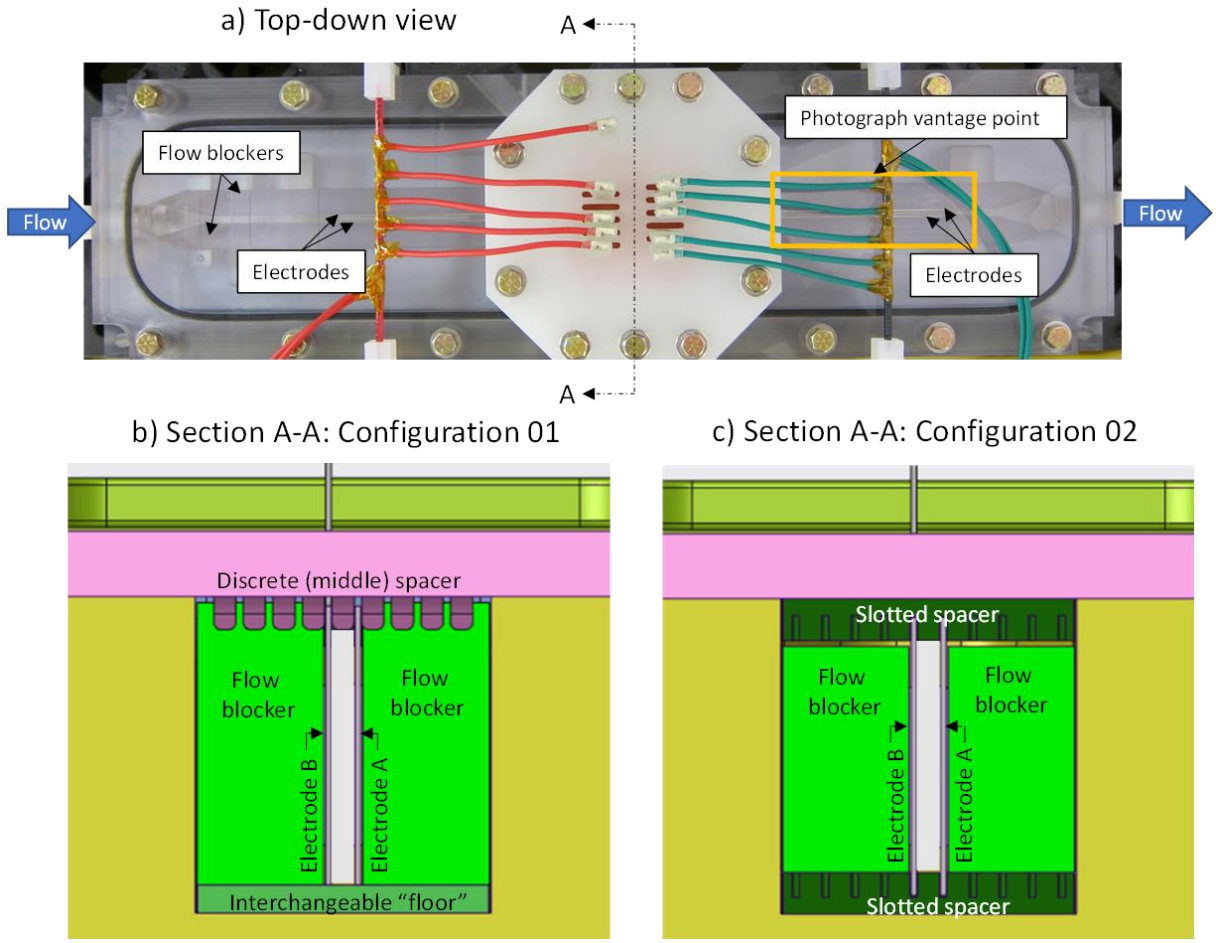

Figure 1. Silver Electrolysis Reactor Proof-of-Concept Prototype. *a) Top-down photograph of reactor; orange box is the approximate vantage point for the photograph in Figure 5 (the green electrical leads were repositioned out of the field of view for that photograph); b) Spacer Configuration 01; c) Spacer Configuration 02. In each image, the reactor is depicted in the two-electrode configuration.*

removed for analysis and polishing. In combination with the interchangeable spacing components, this arrangement also permits the reactor to be placed in alternate configurations with varying numbers of electrodes and electrode spacing. All tests described in this paper were conducted with a 0.25 cm electrode spacing. For reactor configurations with less than the maximum number of electrodes, flow blockers were placed between the walls of the reactor cavity and the outermost electrodes to force all the flow between the electrodes. There are also two possible configurations of the electrode spacers (interelectrode material): 01) discrete spacers at the inlet, middle, and outlet of the reactor and an interchangeable "floor" (flat sheet on which the electrodes rest) or 02) spacers that span the length of the reactor and contain slots into which the electrodes fit. Although Configuration 02 is generally preferred due to the improved consistency in electrode spacing and top/bottom symmetry of the flow channels, Configuration 01 is ideal for testing alternate interelectrode materials because the interchangeable floor could be swapped out with another material without needing to perform any machining to add slots. Thus, Configuration 01 was used for the Alternate Interelectrode Material Test whereas Configuration 02 was used for all other tests. The reactor and its spacer configurations are shown in Figure 1 and the spacer configuration used in each test is listed in Table 2.

Prior to each test case, any wetted components of the reactor (other than electrodes) that had silver deposits from prior testing were soaked in 10% nitric acid and gently scrubbed with a soft-bristle nylon brush to remove deposits. All wetted reactor components (other than electrodes) were then wiped with an ethanol-soaked cotton ball and rinsed thoroughly with deionized water. The electrodes were hand-polished to a 1 micron finish, sonicated in a 1% solution of laboratory-grade detergent, wiped with an ethanol-soaked cotton ball, then rinsed thoroughly with deionized water. In certain test cases, the edges of the electrodes were masked with either electroplating tape or a permanent coating of parylene-C. In both cases, the edge-masking was performed after the aforementioned polishing and cleaning was completed. The parylene-C was applied by Specialty Coating Systems to a thickness of 0.0008" to 0.002" (0.02 to 0.05 mm) using silane A-174 as an adhesion promoter. An image of the electrodes after coating and before electrolysis is shown in Figure 2.

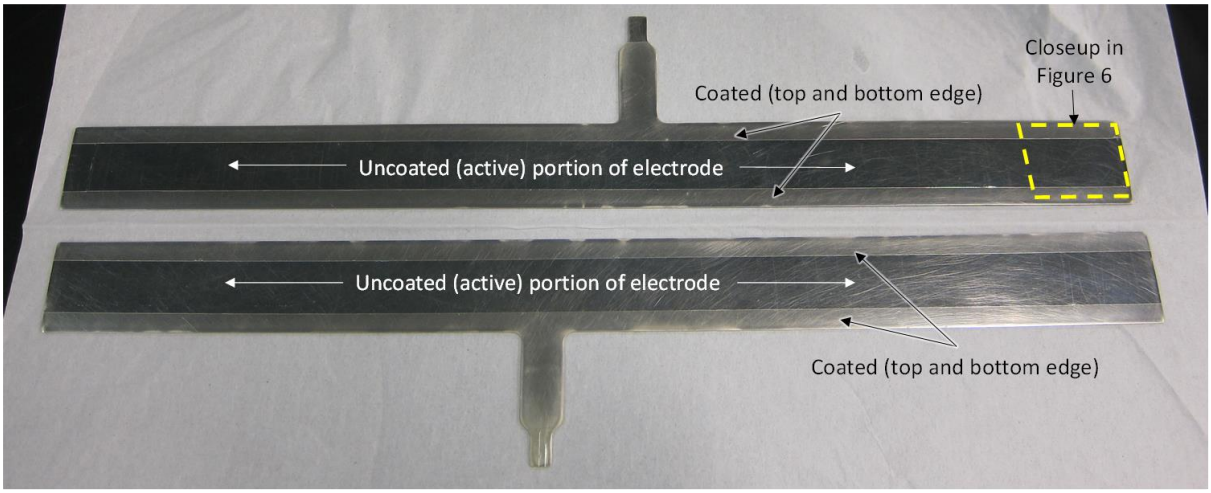

Figure 2. Electrodes: edges coated with parylene-C.

B. Test Rig

The test rig is the same as that described in previous papers with the addition of a dissolved hydrogen sensor (Unisense H_2 microsensor, low-range). Figure 3 shows the test rig with all available components. Components in dashed boxes are optional and were not used in all tests. The dissolved oxygen removal hardware (dashed box A) enables control of the dissolved oxygen concentration in the reactor influent from ~0 to ~8.7 mg/L by adjusting the flow through the dissolved oxygen removal bed (DORB). When this hardware is omitted, the influent dissolved oxygen concentration is approximately 8.7 mg/L (saturated with respect to atmosphere). The ion exchange (IX) beds (dashed box B) provide an ultrapure influent to the reactor by removing the carbonate species present in the water due to dissolution of carbon dioxide from the atmosphere. When included, the influent pH is approximately neutral and the influent conductivity ranges from 0.07 to 0.09 µS/cm. When omitted, the influent water is saturated with atmospheric carbon dioxide, representing a system open to atmosphere and resulting in an influent pH of approximately 5.6 and conductivity of approximately 0.8 to 1.1 µS/cm. The dissolved hydrogen sensor with

accompanying temperature sensor (dashed box C) enables measurement of effluent dissolved hydrogen concentration. When included, the tubing between the reactor outlet and the hydrogen/temperature sensor is replaced with rigid PEEK tubing to minimize loss of any evolved hydrogen. The silver ion-selective electrode (ISE) and pH sensors (dashed box D) enable in-line measurement of silver concentration and pH. The "Test Rig Includes" column in Table 2 indicates the test rig configuration used for each test, where the letters A, B, C, and D indicate which components in dashed boxes in Figure 3 were included with the base configuration. DO1(2) and κ1(2) represent dissolved oxygen and conductivity sensors (respectively), which are part of the base configuration.

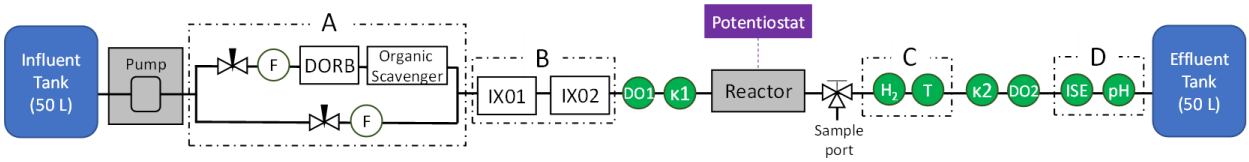

Figure 3. Functional Schematic of Test Rig. *White boxes denote resin beds. Green circles denote sensors. Components for hazard controls or environmental protections are not depicted. The dashed boxes indicate optional components, as discussed in the text.*

C. Test Execution

Inline sensors were calibrated weekly. Water samples were periodically retrieved from the sample port (Figure 3) during operation and analyzed for silver concentration using triplicate measurement of an offline ion selective electrode (ISE: Thermo Scientific 9616BNWP). Silver concentration was also determined by the inline ISE and indirectly using the effluent conductivity sensor (κ2) as described in Reference 1. Because of difficulty in obtaining consistent calibrations with the inline ISE (especially at the lower flowrate of 33 mL/min), the indirect determination of silver concentration from effluent conductivity was generally more reliable than the inline ISE. This determination of silver concentration, indicated by Ag_k, is the method used in this paper for reporting inline silver concentration. Other aspects of test execution that were specific to a given test are outlined in Table 2. Tests that used only two electrodes were essentially emulating a single cell of what would be a multi-cell reactor; thus, for these tests, the flowrate was reduced from the nominal 100 mL/min. However, because of constraints on the test rig, the flowrate could not be reduced below 33 mL/min, which ultimately results in a higher current density (generally three times that of the ten-electrode configuration). This is beneficial in that the two-electrode configuration can be seen as a worst-case condition, which helped to identify trends and accelerate testing.

1. *Alternate Interelectrode Material Test*

For the Alternate Interelectrode Material Test, three different materials were used for the interchangeable floor: polycarbonate (PC), polytetrafluoroethylene (PTFE), and quartz. Two cases were conducted with each material: one with constant polarity ("Alt. Intelec. Matl. 01" in Table 2) and one with polarity reversed on a 1-minute half-cycle ("Alt. Intelec. Matl. 02" in Table 2). For the first case, the system was run to failure (electrode bridging fault). Three replicates were performed for PC and quartz; that is, three distinct floor components of that material and three distinct sets of electrodes were tested independently. Due to time constraints, only one replicate was performed for PTFE. For the second case, the system was run for 24 cumulative hours. Only one replicate of each material was performed in the second case.

2. *Coated Edge Test*

For the Coated Edge Test, the system was run for 146 cumulative hours, which treats the amount of water consumed by one crewmember in a year. In this test, samples of both the influent and effluent of the reactor were taken each day: one prior to initiating electrolysis and one in the middle of the day (about four hours into the electrolysis). The influent samples were obtained by disconnecting the tubing between κ1 and the reactor and retrieving a sample from the effluent of κ1. In addition to measuring silver concentration, the samples were also analyzed for organic and inorganic contaminants via total organic carbon (TOC) and ion chromatography (IC). Prior to the test, the reactor was flushed with DI water for a cumulative ten hours (two hours per day for five days) and both influent and effluent were sampled at 0, 0.5, 1, and 2 hours each day in order to test the water quality. No electrolysis was performed during this flushing period. For the first two days, the electrodes were omitted from the reactor assembly in order to determine the baseline TOC release from the other wetted materials. Then, for the latter three days, the electrodes were included in the assembly to determine if the electrode edge coating increased the TOC release. This flush period also provided the baseline with which to compare the TOC release during operation. The current for this test was initially (for the first four hours) set to 0.7 mA to be consistent with the polarity reversal test

from last year's paper.[2] However, it was determined that the enhanced current efficiency provided by the edge masking in this case yielded a significantly higher silver concentration, so the current was reduced to 0.5 mA at hour four (this yielded a silver concentration slightly higher than 400 ppb) and was kept at that value for the duration of the test. The final flight system will be operated such that the silver output is closer to the middle of the 200–400 ppb range (e.g. 300 ± 50 ppb). Operating at the high end of the range is more demanding on the reactor and thus serves as a better test of performance.

3. Cathode Reaction Test

The Cathode Reaction Test consisted of three test cases with different combinations of number of electrodes and current (see Table 2). These test cases are referred to as "Cathode Reaction 01(2,3)" in Table 2 and "CR01(2,3)" in Figure 7. In Cathode Reaction Test 01, the current was set to 0.75 mA (current density of 1.4 μA/cm^2) because it resulted in the target silver concentration of ~400 ppb. In Cathode Reaction Test 02, the current was set to 3.0 mA (current density of 5.5 μA/cm^2), the maximum permissible current based on constraints of the test rig. The rationale for using the maximum current was to accentuate the DO consumption and make associated trends more apparent. In Cathode Reaction Test 03, the current was returned to 0.75 mA, but the number of electrodes was reduced to two in order to maximize the current density (12.4 μA/cm^2). Each test case comprised multiple steps at varying influent DO concentration. Each step was a distinct experiment consisting of a stabilization period (to allow the DO concentration to reach its new steady-state value) followed by thirty minutes of electrolysis at the test current. The DO concentration was controlled by varying the percentage of flow bypassing the dissolved oxygen removal bed (DORB) versus flowing through it. Electrode polarity was constant during each step but reversed between steps. In each step, the bias between the influent and effluent DO sensors was determined just prior to the initiation of electrolysis, and this bias was subtracted from the steady-state difference between the sensors to give the DO consumption. System performance was assessed by comparing the steady-state voltage, silver concentration, DO consumption, and dissolved hydrogen concentration at the various influent DO concentrations.

4. Elevated Concentration Test

The Elevated Concentration Test consisted of two test cases: one with the ion-exchange beds included in the test setup to provide "Ultrapure" influent to the reactor ("Elevated Conc. 01" in Table 2), and a second case with the ion-exchange beds omitted to provide "Atmosphere-Equilibrated" influent ("Elevated Conc. 02" in Table 2). In both cases, the current was increased by 1.5 mA every thirty minutes. Polarity was reversed with each current increase but was otherwise constant during the thirty-minute current increment. Samples were taken in the last five minutes of each current increment and analyzed for silver concentration.

III. Results

A. Alternate Interelectrode Material Test

Table 3 provides a summary of the results for this test. It also lists the results of two prior test cases that were performed in reactor spacer configuration 02 for the sake of comparison.

Table 3. Alternate Interelectrode Material Test Results

Material	Spacer Config	Polarity Reversal	Current (mA)	Avg†† Ag+ (ppb)	Current Efficiency	Time to Failure (hrs)	Deposit observations
PC*†	02	N/A	0.33	320	48%	1.9	Dendritic; bridged gap; solidly adhered
PC†	01	N/A	0.33	430	64%	5.4	Dendritic; bridged gap; solidly adhered
Quartz†	01	N/A	0.33	310	46%	3.5	Dendritic; bridged gap; solidly adhered
PTFE	01	N/A	0.33	240	36%	1.3	Dendritic; bridged gap; washed away easily
PC*	02	1 min	0.70	420	N/A	N/A	Along electrode interface only; see Ref. 2
PC	01	1 min	0.70	320	N/A	N/A	Very minor; almost impercetible
Quartz	01	1 min	0.70	410	N/A	N/A	Very minor; almost impercetible
PTFE	01	1 min	0.70	460	N/A	N/A	Very minor; almost impercetible

*From prior testing; included for comparison

†Results listed are the average of three replicates; all other cases were a single replicate

††Average silver concentration is an estimated average of the steady-state concentration throughout the test case

The first four cases, which were the constant polarity cases, all failed within a few hours and three had current efficiencies less than 50%. Given the fact that the reactor was intentionally operated in a worst-case condition to accelerate failure, this is not alarming. Rather, it establishes that although there were some differences in performance based on the use of different interelectrode materials, this change alone was not sufficient to prevent the bridging fault. It is also interesting to note that the materials that were expected to perform better at preventing deposits (quartz for its low porosity and PTFE for its low surface energy) actually appear to perform worse in the constant polarity mode of operation, as evidenced by the lower current density and shorter time to failure compared to polycarbonate (PC) in the same spacer configuration. Conversely, it appears that the alternate materials did offer an advantage when coupled with polarity reversal. Operation with polarity reversal at a one-minute half-cycle prevented electrode bridging throughout the 24 hours cumulative operation in all cases regardless of interelectrode material. However, the silver output was lowest for polycarbonate (PC) and highest for PTFE. (Although polarity reversal prevents a straightforward determination of current efficiency, the silver concentration serves as a performance metric to be compared from one case to another.) The reason for the reversal in material performance between constant and reversed polarity is not clear; additional replicates would need to be gathered to arrive at a conclusion. Perhaps the more important observation from the polarity reversal cases is contained in the far right column of the table. Namely, it appears to have been the spacer configuration, rather than the interelectrode material, that had a larger contribution to the prevention of silver deposits on the interelectrode material. In Configuration 02, the slot in the spacer is slightly wider than the electrode to provide clearance, but the very narrow gap between the surface of the electrode and the edge of the slot results in stagnant electrolyte that may allow a buildup of electrolysis products. The absence of the slot in Configuration 01 could explain its improvement in deposit prevention. Again, further replicates would be needed to arrive at a conclusion. In any case, this testing further demonstrated the positive effect of polarity reversal in preventing electrode bridging.

B. Coated Edge Test

The key parameters of interest from the Coated Edge Test are plotted in Figure 4. The data show that the reactor was able to provide silver at a concentration near the target value of 400 ppb for at least 146 cumulative hours of operation, which is equivalent to treatment of the amount of water consumed by one crewmember in one year (thus, one crew-year of water). The offline ISE data ranges from 394 to 434 ppb. Ignoring the higher concentration and voltage observed during the first four hours when the current was 0.7 mA rather than 0.5 mA, the values of these parameters are relatively consistent throughout the one crew-year cumulative timeframe of the test. There is an overall gradual decrease in both the silver concentration and the pH ($[OH^-]$ is proportional to $[Ag^+]$; see Ref. 1). Meanwhile, there is an overall slight increase in the end-of-half-cycle voltage for both polarities. The magnitude of these changes is not problematic, but silver concentration and voltage have generally been even more consistent in past testing. In any case, in future testing, it will be important to monitor these parameters to establish any long-term trends over the full targeted life of the system (12 crew-years).

The test also demonstrated that the combination of polarity reversal with masked electrode edges provided optimal performance. Whereas past testing with polarity reversal alone resulted in silver deposits along the edges of the electrodes and edge-masking alone resulted in cathodic flakes,[2] the combination of the two techniques eliminated the flakes and reduced the silver deposits to the point that they were barely detectable with the naked eye. This performance is evidenced in Figure 5, a photograph of the electrode gap upon completion of the test, which is consistent with photographs taken every hour during the test.

Finally, the test determined that parylene-C is an appropriate coating for the electrode edge-masking application. In addition to the good performance of the reactor from a silver output perspective, the reactor also behaved well in terms of contaminant leaching. In fact, only during the initial reactor flush without the electrodes was there any measurable TOC (above the detection limit of 250 ppb) in the effluent samples. The TOC from the initial reactor flush may have simply been a release of residual ethanol from the reactor cleaning procedure. During the flush with electrodes and during the operational period, none of the effluent samples had any measurable TOC nor any measureable ionic contaminants (above the IC detection limit of 500 ppb). Finally, comparison of pretest and posttest electrode photographs indicates that there was no macroscopically observable delamination or degradation of the coating (see Figure 6). The change in color from shiny silver to dull beige/gray demonstrates that the active surface has clearly undergone significant change, whereas the coated substrate has maintained its pristine form. Furthermore, close inspection of the line between coated and active surfaces along both electrodes revealed no evidence of degradation. All of the data and observations point to the conclusion that masking the electrode edges with parylene-C provides reliable, long-duration performance with no negative impact on the product water or the coating itself. It is

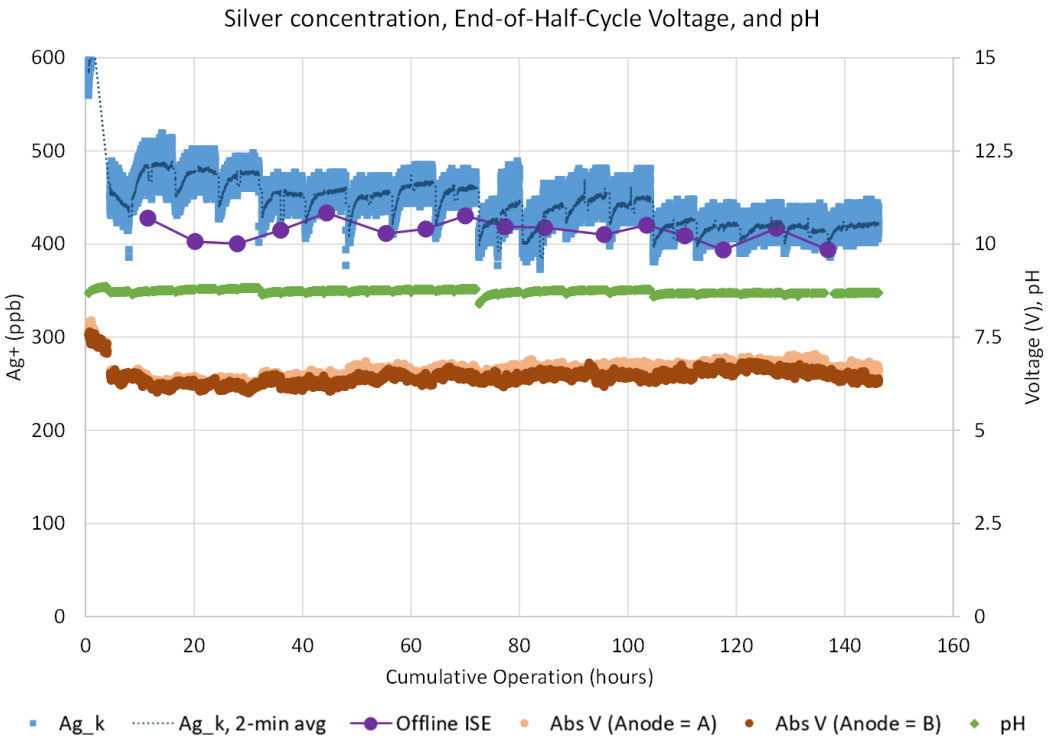

Figure 4. Coated Edge Test Data. *Silver concentration (Ag_k and Offline ISE) is plotted on the left axis, voltage and pH on the right. The 2-minute average of Ag_k indicates the average silver concentration of a full cycle of polarity reversal and smooths out the periodic fluctuations that result from polarity reversal and look like scatter in the raw Ag_k data. The plotted voltage is the absolute value of the end-of-half-cycle voltage from each half-cycle. The voltage is plotted in two series to distinguish the "forward" and "reverse" half-cycles. Inline data (Ag_k, voltage, and pH) taken during sampling and system startup is omitted.*

Figure 5. Photograph of Electrode Gap. *Photograph taken upon completion of the Coated Edge Test from the vantage point indicated in Figure 1a.*

thus reasonable to incorporate edge-coated electrodes into the next generation design, which will be tested for a full mission duration.

Figure 6. Electrode A: Pre/Posttest Comparison. *Photographs of the downstream end of Electrode A before and after Coated Edge Test.*

C. Cathode Reaction Test

Figure 7 shows the oxygen consumption and hydrogen evolution from the three test cases in the Cathode Reaction Test. The steady-state values of these parameters from each step in influent dissolved oxygen (DO) concentration is plotted in order to show the extent to which these reactions take place as a function of influent DO. First, the hydrogen concentration plot confirms the hypothesis that it is indeed hydrogen evolution that takes over as the primary cathode reaction at very low influent DO concentrations (less than ~1 mg/L). Second, it is clear that when the influent DO is above a certain threshold (~2 mg/L in this case), not only is oxygen reduction the primary reaction, but also hydrogen evolution does not take place even as a secondary reaction.

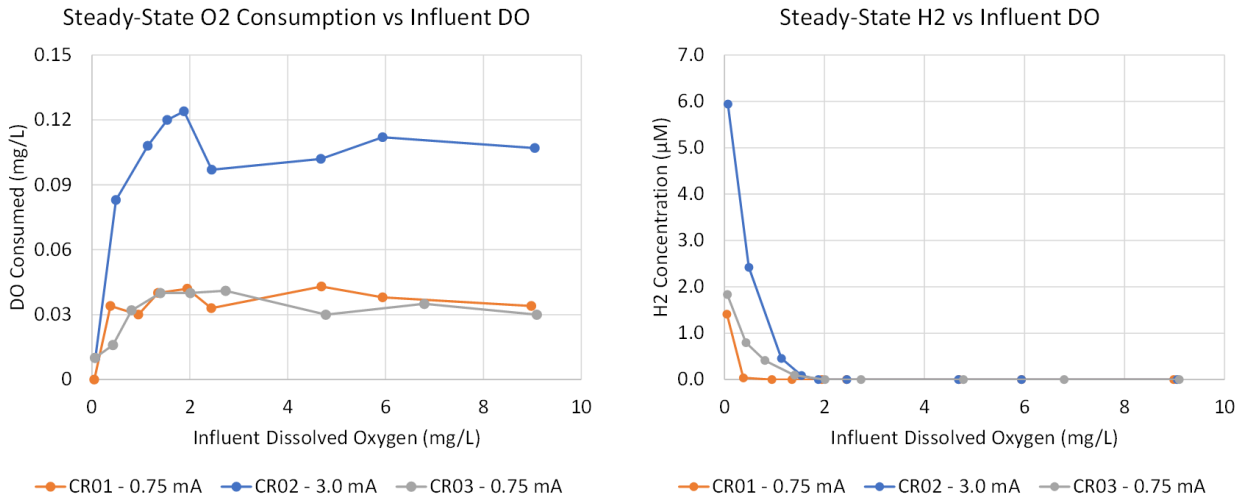

Figure 7. Oxygen Consumption and Hydrogen Evolution.

Further insights are made available by thinking about each reaction in terms of its current fraction, φ_i, which is the fraction of the total electrode current, I_T, that goes toward that reaction.

$$\varphi_i = \frac{I_i}{I_T} \tag{1}$$

The current consumed by a particular reaction, I_i, is determined by Faraday's law and the measured change in concentration, C_i, of reactants or products for that reaction:

$$I_i = \nu_i F C_i \forall \quad (2)$$

where ν_i is the stoichiometric ratio of electrons to species *i* in the reaction, *F* is Faraday's constant, and $\forall$ is volumetric flowrate.

The sum of the current fractions at an electrode is one (see Table 1 for the reaction abbreviations used in the current fraction subscripts):

$$\text{Cathode: } \varphi_{O2} + \varphi_{H2} + \varphi_{Ag\_dep} = 1 \quad (3)$$

$$\text{Anode: } \varphi_{Ag2O} + \varphi_{Ag+} = 1 \quad (4)$$

The current fraction of silver deposition at the cathode and oxide formation at the anode are of interest because these are the known contributions to less-than-ideal current efficiency for the silver dissolution reaction. Silver oxide formation competes with silver dissolution for anodic current, as seen in Eq. (4). Cathodic silver deposition reduces the effluent silver concentration and thus reduces the apparent anodic current efficiency of the silver dissolution reaction, such that the measured silver dissolution current fraction, $\varphi_{Ag+,meas}$, is a portion of the actual:

$$\varphi_{Ag+,meas} = \varphi_{Ag+} - \varphi_{Ag\_dep} \quad (5)$$

Eqs. (3) – (5) can be used to determine the unknown (not measured) current fractions based on the measured current fractions. First, Eq. (3) is used to determine φ_{Ag_dep} from the measured values of φ_{O2} and φ_{H2}. Then Eq. (5) is used to determine φ_{Ag+}, and Eq. (4) is used to determine φ_{Ag2O}. In this way, the full understanding of the cathode reactions provided by hydrogen measurement (in addition to DO measurement) provides important insight into the anode reactions. This is exemplified in Figure 8, which shows the current fraction for each reaction at each influent dissolved oxygen concentration in Cathode Reaction Test 02.

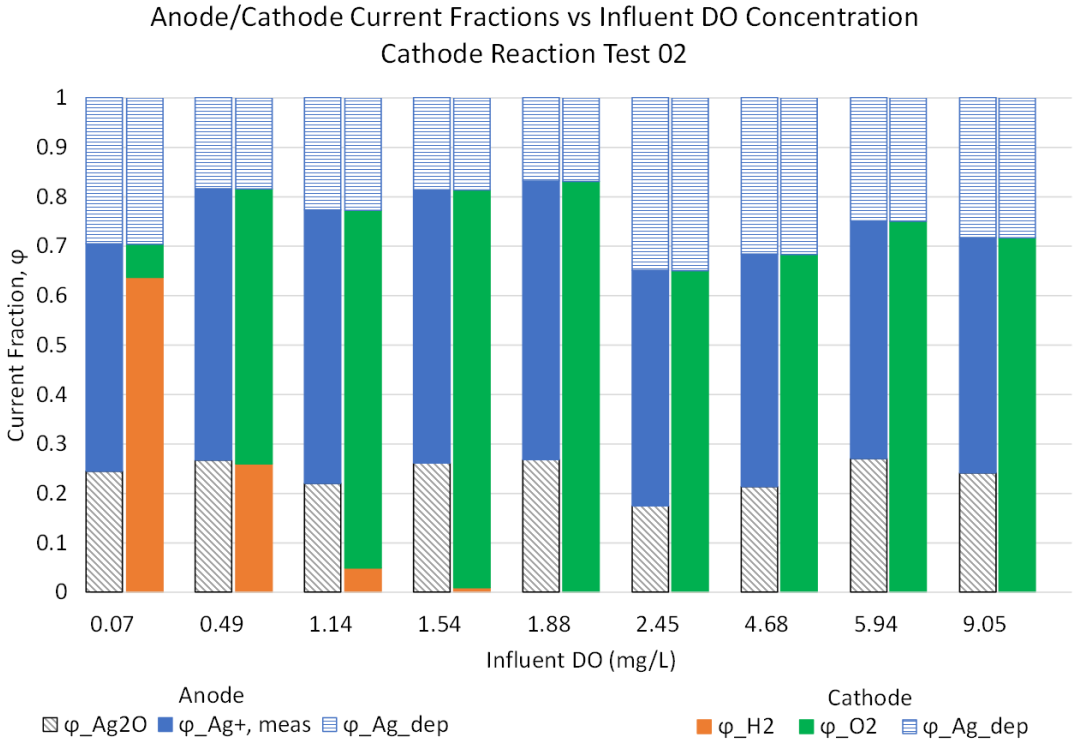

Figure 8. Current Fractions from Cathode Reaction Test 02. *Each bar color/style represents one of the two anode reactions or one of the three cathode reactions (see Table 1). Solid shading denotes current fractions that are determined by concentration measurement, whereas patterned shading (horizontal or diagonal hatches) denotes current fractions that are determined by calculation. Each pair of bars depicts the current fractions (anode on left, cathode on right) at each influent dissolved oxygen concentration.*

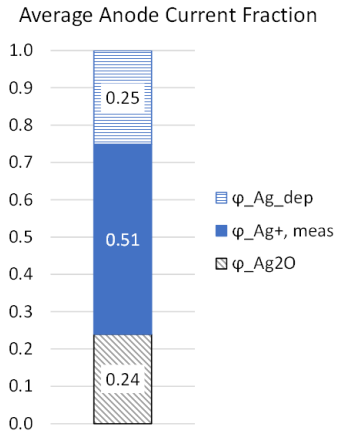

Figure 9. Average Anode Current Fractions in Cathode Reaction Test 02.

The consistency of the sum of φ_{O2} and φ_{H2} indicates that the other current fractions are not dependent on DO concentration. On average, that sum was 0.75, which means that the average silver deposition current fraction was 0.25. The measured silver concentration was also consistent, and the average $\varphi_{Ag+,meas}$ was 0.51. Thus, anodic oxide formation accounted for 24% of the anodic current, on average (see Figure 9). The current fractions of the various reactions are strongly dependent on the specific conditions of the test: current (and thus effluent silver concentration and pH), reactor configuration, influent water condition, etc. An understanding of current fractions and how they are impacted by operational conditions sheds light on which reactions contribute to inefficiencies and enables optimization of the silver dissolution current efficiency. Although the present performance of the system is adequate to meet mission objectives, optimization of current efficiency enables minimization of reactor size, which increases the competitiveness of the technology when traded against other biocide dosing options.

D. Elevated Concentration Test

The ability to increase the concentration by simply turning up the current makes the electrolysis technology very versatile. This capability has important applications including the ability to increase potable bus silver concentration going into dormancy and to create solutions for microbial shock of contaminated systems. In the Elevated Concentration Test, shown in Figure 10, nearly an order of magnitude increase over the nominal concentration was achieved with both ultrapure and atmosphere-equilibrated influent. The difference between the two curves, however, is significant. In the case of ultrapure water, the reactor appears to reach a maximum silver output of about 1800 ppb, whereas in the case of atmosphere-equilibrated water, the silver concentration reaches approximately twice that value and has yet to max out. This can be explained by the fact that the atmosphere-equilibrated water, by virtue of its carbon dioxide content, has a lower pH (about 5.6 versus 7.0). The lower pH discourages the anodic oxide formation reaction (see Table 1), which is a significant contributor to the loss of current efficiency (as discussed in the previous section). This points to the possibility of significantly increasing current efficiency by aerating the influent water, if future water system architectures allow such a modification. In either case, as more silver is produced, the pH increases, which in turn increases the favorability of the oxide formation reaction. This is why the current efficiency decreases with increasing current. Nevertheless, even the silver concentration achieved with the ultrapure water may be sufficient for a microbial shock. If not, the maximum concentration could be improved by reactor geometry optimization.

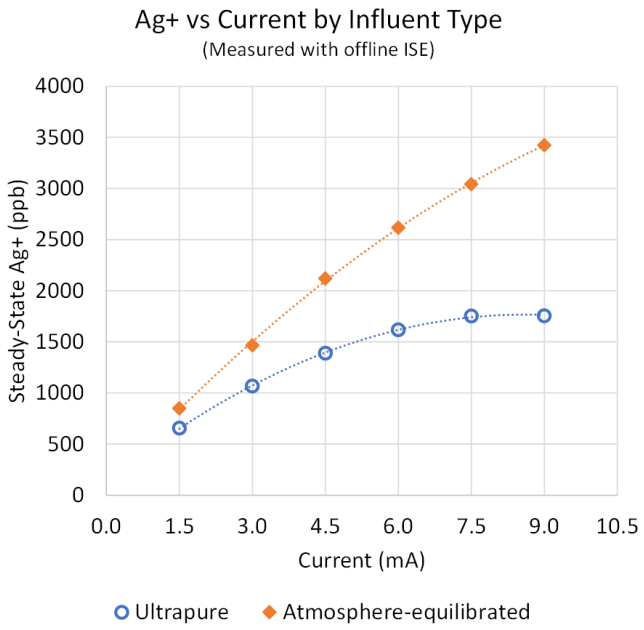

Figure 10. Elevated Concentration Test. *Data points are the silver concentration of the samples taken at the end of each current increment. Dotted lines are quadratic curve fits of the data.*

IV. Conclusions and Future Work

Silver electrolysis testing in the past year consisted of four sets of tests. The Alternate Interelectrode Material Test indicated that interelectrode material properties do not have a significant enough effect on silver deposit formation to be relied upon for prevention of electrode bridging. The test also suggested that electrode spacer configuration is a more significant contributor to deposit formation and further demonstrated that polarity reversal is a key component in an electrode bridging prevention strategy. The Coated Edge Test demonstrated the benefit of coupling electrode edge masking with polarity reversal in the bridging prevention strategy, which enabled at least one crew-year of operation while maintaining very clean electrode spacers. The test also showed that parylene-C is an effective and appropriate coating for this application. The Cathode Reaction Test confirmed the hypothesis that hydrogen evolution is evolved at very low influent dissolved oxygen concentrations. The test also showed that hydrogen evolution is limited to those low DO concentrations and does not occur under normal circumstances. Furthermore, analysis of the current fractions of the cathode reactions provides insight into the reactions taking place at the anode, which will help in optimizing the silver production current efficiency. Finally, the Elevated Concentration Test demonstrated the reactor's ability to achieve silver concentrations approximately an order of magnitude greater than the nominal concentration, which can be exploited both for system dormancy prep and microbial shock. In addition to the testing, advances were also made on the reactor multiphysics model, which will be reported in a future publication. The knowledge gained from each of these efforts is being applied to the design of a next-generation prototype that will be used to characterize the effectiveness and reliability of the technology for long-duration space missions.

Acknowledgments

The authors would like to thank the Exploration Capabilities, Life Support Systems Project for their support of this research as well as the countless colleagues who provided advice, sample analysis, assistance with reactor design and test rig development, and editorial suggestions.

References

[1] P. Hicks and N. Adam, "Feasibility Testing of Silver Electrolysis for Disinfection of Spacecraft Potable Water Systems," in *International Conference on Environmental Systems*, St. Paul, 2022.

[2] P. Hicks, R. Garcia Fernandez and N. Adam, "Silver Electrolysis for Disinfection of Spacecraft Potable Water: 2023 Update," in *International Conference on Environmental Systems*, Calgary, Canada, 2023.

[3] R. Garcia Fernandez, S. Marshall and N. Adam, "Material Compatibility Study of Coated Metals to Maintain Biocidal Silver in a Spacecraft Potable Water System," in *International Conference on Environmental Systems*, Calgary, Canada, 2023.

[4] J. Vance and L. Delzeit, "Mitigation of Silver Ion Loss from Solution by Polymer Coating of Metal Surfaces, Part II," in *International Conference on Environmental Systems*, 2020.

[5] J. Vance and L. Delzeit, "Mitigation of Silver Ion Loss from Solution by Polymer Coating of Metal Surfaces, Part III," in *International Conference on Environmental Systems*, 2021.

[6] J. Vance and L. Delzeit, "Mitigation of Silver Ion Loss from Solution by Polymer Coating of Metal Surfaces, Part IV," in *International Conference on Environmental Systems*, Saint Paul, MN, 2022.

[7] J. Vance and L. Delzeit, "Mitigation of Silver Ion Loss from Solution by Polymer Coating of Metal Surfaces, Part V, and Related Developments," in *International Conference on Environmental Systems*, Calgary, Canada, 2023.

[8] Specialty Coating Systems, "SCS Parylene Properties," [Online]. Available: https://scscoatings.com/parylene-coatings/parylene-properties/. [Accessed 5 April 2024].

[9] P. Delahay, M. Pourbaix and P. Van Resylberghe, "Potential-pH Diagram of Silver," *Journal of the Electrochemical Society*, pp. 65-67, February, 1951.